applied sciences

MDPI

Article

Analysis of Fatigue Performance of Spot-Welded Steel T-Profiles Under Cyclic Torsional Loading

Murat Demiral [1,*] and Ferhat Kadioglu [2]

[1] College of Engineering and Technology, American University of the Middle East, Egaila 54200, Kuwait
[2] Department of Aerospace Engineering, Ankara Yildirim Beyazit University, Ankara 06010, Türkiye; ferkadioglu@gmail.com
* Correspondence: murat.demiral@aum.edu.kw

Abstract: Steel T-profiles with the spot-welding manufacturing process are extensively used in various sectors such as construction, automotive, renewable energy, etc., due to their versatility and reliability. These profiles are exposed to various loading modes during their service life, which include axial, bending, shear, torsional, or combinations thereof. This paper investigates the fatigue performance of a spot-welded T-profile assembly subjected to torsional cyclic loading. The extended finite element method (XFEM) analysis was performed to simulate the intricate behavior of spot welds under the loading, elucidating critical areas prone to fatigue initiation and propagation especially around the spot welds. The simulation results were compared with previously obtained experimental results. Both results are consistent. The effects of various parameters, including the spot-weld diameters, the amount of torque applied, thickness of the profile parts, and the presence of base part, on the fatigue performance of the assembly were studied critically.

Keywords: diameter of the spot weld; load ratio; number of spot welds; spot-welded box; torsional fatigue loading; XFEM

check for updates

Citation: Demiral, M.; Kadioglu, F. Analysis of Fatigue Performance of Spot-Welded Steel T-Profiles Under Cyclic Torsional Loading. *Appl. Sci.* **2024**, *14*, 10607. https://doi.org/10.3390/app142210607

Academic Editors: Andrea Sellitto and Angela Russo

Received: 15 October 2024
Revised: 3 November 2024
Accepted: 15 November 2024
Published: 18 November 2024

Copyright: © 2024 by the authors. Licensee MDPI, Basel, Switzerland. This article is an open access article distributed under the terms and conditions of the Creative Commons Attribution (CC BY) license (https://creativecommons.org/licenses/by/4.0/).

1. Introduction

Steel T-profiles are essential for a wide range of industries. They are crucial components of structural frameworks, support beams, and trusses used in construction, ensuring the durability and strength of buildings, bridges, and industrial facilities [1]. Due to their rigidity and capacity to support loads, these profiles are vital in the production process for constructing machine frames and equipment supports. In the transportation sector, they provide structural support for train tracks, bridges, and tunnels, particularly in areas experiencing dynamic loads. Additionally, they reinforce chassis construction in automotive applications, enhancing vehicle longevity and safety. These profiles are also widely utilized in renewable energy systems, agricultural, maritime engineering, and infrastructure projects, indicating their versatility and dependability across various industries.

Spot welding is one of the techniques used to produce T-profiles, especially when fabricating structural and automotive components [2]. The initial steps in the procedure involve preparing the steel sheets, cutting them to size, and ensuring their cleanliness. T-profiles are then created by spot welding perpendicular sheets together.

Steel T-profiles can be subjected to various types of loadings such as torsional, axial, bending, shear, or a combination, depending on the application and environmental conditions [3]. Torsional loading involves twisting forces applied to the T-profile about its longitudinal axis. This kind of loading is frequently seen in situations where the T-profile is twisted or rotated, such as in car chassis during cornering or in structural frameworks subjected to seismic or wind pressures. When exposed to cyclic torsional loadings, steel T-profiles face many challenges, especially in structural frameworks and automotive chassis applications. These challenges must be addressed to prevent fatigue failure resulting from

repetitive twisting forces. Thus, fatigue resistance is crucial. By uniformly distributing torsional loads throughout the cross-section, a well-designed structure extends the fatigue life of T-profiles and reduces stress concentrations that can cause premature failure. Innovative design approaches, such as refining the cross-sectional form and including reinforcement features, are used to optimize T-profiles for better fatigue resistance.

In the literature, a few studies have focused on the cycling performance of spot-welded structures. Kardomateas [4] predicted the cyclic endurance of spot-welded connections in beams subjected to both bending and torsional forces, analyzing the physical mechanisms associated with stress induced by buckling. A two-dimensional model of buckling was employed to determine the stress distribution. Janardhan et al. [5] conducted high-cycle fatigue tests to examine the failure mechanisms of resistance spot-welded DP600 steel. This study revealed that fatigue crack initiation predominantly occurred in the heat-affected zone or near the fusion zone. Subsequently, fatigue crack propagation extended through both the thickness and width directions until final failure. The primary factors affecting the failure mechanism of spot welds under fatigue loading were the stress concentration at the junction of the two bonded sheets, the stress intensity factor, and the base metal's strength. Ertas and Akbulut [6] conducted a series of fatigue life tests on modified tensile shear (MTS) test specimens joined by spot welding to investigate the impact of electrode force on fatigue life. The experimental results revealed that the number of cycles until failure varied depending on the spot-welding configurations, including electrode force and welding schedules. Their results suggested that through-thickness cracking was the main characteristic associated with fatigue failure. Duran and Demiral [7] analyzed high-cycle fatigue of spot welds using the extended finite element method (XFEM) and finite element method (FEM). The advantage of XFEM simulations was the ability to observe the fracture propagation path, although the simulation time of FEM-based fatigue assessments was noticeably less. Qian et al. [8] tested Al-steel resistance spot-welded T-joint structures under impact loads, conducting both analytical and numerical studies on the fracture behaviors and mechanisms. Aghabeigi et al. [9] compared several fatigue damage criteria to forecast dissimilar friction stir spot welds' fatigue life in cross-tension and lap-shear specimens. The Smith–Watson–Topper criterion showed the least amount of disagreement between experimental data and anticipated fatigue lifetimes, while a high degree of agreement was seen when using the Fatemi–Socie criterion to predict the locations of fracture tips in both types of specimens. Oh and Umewaza [10] used welded elbow pipe and socket specimens and stainless steel sheets to conduct high-cycle fatigue testing under combined loading situations. The features of the welded specimens were studied using the parent sheet's cyclic stress–strain curve. The stress concentration area of the weld experienced Mode I or Mode I + III fatigue fracture, with the crack initiation point varying according to the loading mode. Using the Gough–Pollard failure criterion for analysis, the applied load was divided into bending and torsion, and the fracture began on the side with the higher equivalent stress. Elitas et al. [11] examined bending fatigue in Al 1100-DP steel (LITEC 1050) bimetal, noting that fatigue cracks were not observed at the Al–intermetallic interface but were seen at the interface of Litec DP steel and intermetallic at the site of the explosive weld.

However, none of these studies examined the performance of spot-welded T-profiles under cyclic torsional loads. Understanding the failure mechanisms is crucial for enhancing fatigue resistance and extending the service life of spot-welded assemblies. Accurately predicting the location of damage initiation, its spread with increasing cyclic loads, the failure cycle, and the importance of different assembly components is critical. This study developed an extended finite element (XFEM) model for a spot-welded assembly subjected to torsional loading. Initially, experimental data for two distinct scenarios were used to validate the numerical model. Subsequently, an evaluation was conducted to determine the impact of various model parameters, such as the diameter of spot welds used (D), the amount of torque applied (T), the thickness of the constituent parts of the assembly (t), and the presence of a base part on its fatigue performance.

2. XFEM Modelling

A three-dimensional XFEM model of the spot-welded assembly under torsional loading was created in this study. Abaqus 2021 FE software [12] was used for this purpose. The geometric details of the assembly's component parts are shown in Figure 1. There are four main sections. During fatigue loading, Parts 1 and 2, which are the main parts, are supported by Parts 4 and 3, respectively.

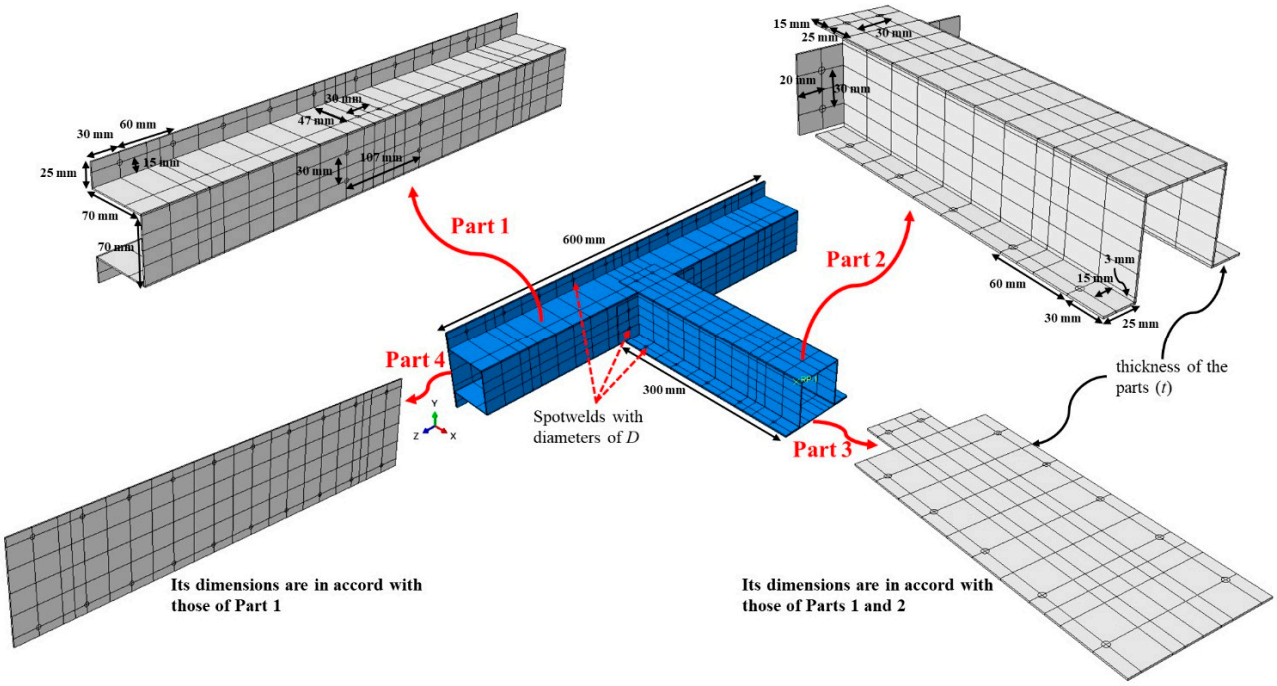


Figure 1. Geometric details of the constituent parts of the T-profile assembly.

Figure 2 presents the details of the developed XFEM model. The assembly was subjected to the torsional loading T from the free ends of Parts 2 and 3 with a length of 75 mm, while it was fixed in all directions from the free ends of Parts 1 and 4 with the identical lengths. T was applied to the reference point depicted in Figure 2, which is situated at the geometric centre of the structure's loaded portion. This point (RP-1) controlled the concerned region by means of the coupling constraint defined in the model. XFEM was primarily specified in these areas of the parts brought together using spot welds, in accordance with studies in the literature demonstrating that the cracks primarily originate and expand around the spot welds joining the structure. Using Abaqus' tie constraint module, the interfaces of the parts on the welding side were set as master and slave surfaces in order to simulate spot welding. To form the assembly, different parts are joined together using a total of 38 spot welds. Twenty of them connected Parts 1 and 4, ten of them for Parts 2 and 3, six spot welds joined Parts 1 and 2, and two spot welds joined Parts 1 and 3 in the end.

Using 25 Fourier terms, a direct cycle analysis was carried out to simulate the fatigue loading with load ratio of -1. To trigger crack formation in the regions of stress concentration, T was applied to the structure in a separate static step prior to the loading cycle.

Details of the mesh used in the model are presented in Figure 2. To ensure accuracy of the model, a mesh convergence study was performed. Three simulations were run when the assembly was subjected to the static T load, using three different mesh sizes: 1.25 mm, 0.625 mm, and 0.3125 mm. The highest von Mises stress value found in the element adjacent to the welding zones was compared from each model. When the mesh size was adjusted from 0.625 mm to 0.3125 mm, the difference of concern was less than 4.13%, and when the mesh was changed from the coarsest to the medium one, it was more

than 10.0%. As a result, the model was discretized using 0.625 mm element sizes. Because XFEM results are independent of the mesh size utilized, it is vital to emphasize that this mesh study was conducted for the static analysis simulating the formation of the cracks. For the discretization, eight-node linear brick elements with reduced integration (C3D8R) were employed.

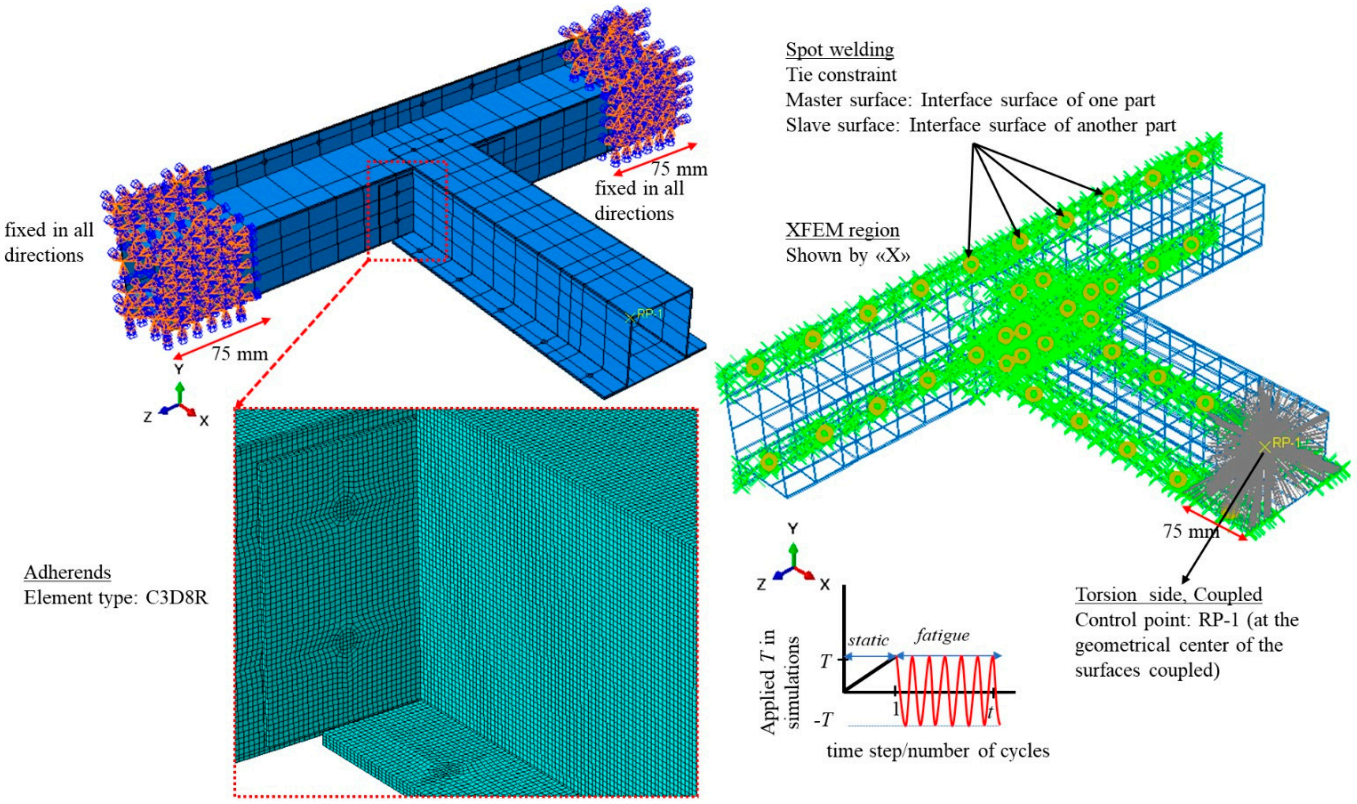


Figure 2. The details about the XFEM modelling of the T-profile assembly subjected to cyclic torsional loading.

The XFEM formulation procedure is summarized in Figure 3. In XFEM, a displacement vector function u with the partition of unity enrichment is approximated as follows:

$$u(x) = \sum_{I \epsilon N} N_I(x) \left[u_I + H(x)\alpha_I + \sum_{\alpha=1}^{4} F_\alpha(x) b_I^\alpha \right] \quad (1)$$

where $N_I(x)$ represents the typical nodal shape functions; u_I, the typical nodal displacement vector associated with the continuous portion of the finite element solution, is the first term in the equation above that appears on the right side. Multiplying the nodal enriched degree of freedom vector (a_I) by the corresponding discontinuous jump function $H(x)$ over the fracture surfaces yields the second term in the equation. The nodal enriched degree of freedom vector, b_I^α, and the associated elastic asymptotic crack-tip functions, $F_\alpha(x)$, are multiplied to obtain the third term. In this case, the first term on the right covers every node in the model; the second term only covers nodes whose shape function support is cut by the crack interior; the third term only covers nodes whose shape function support is cut by the crack tip.

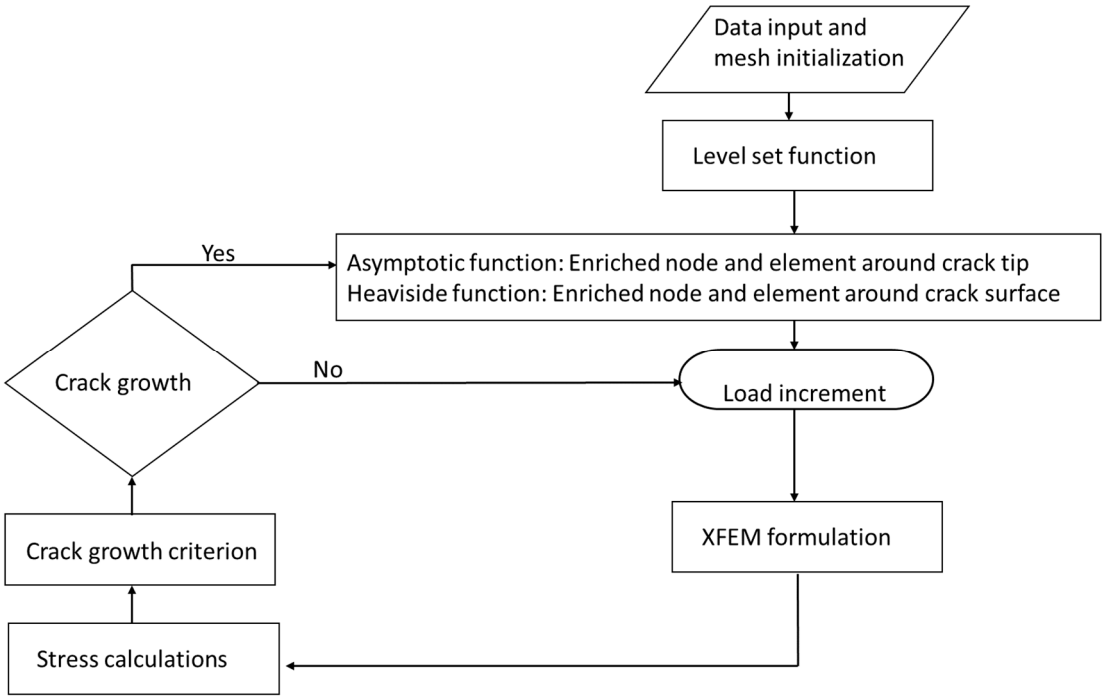


Figure 3. XFEM flowchart [12].

The simulations employed the direct cyclic approach in Abaqus 2021/Standard, combining the XFEM and linear elastic fracture mechanics (LEFM). The crack's nucleation and evolution were modeled using the Paris law, which relates the fracture energy release rate to crack growth. G_{pl} = 0.85 $G_{eq,\,c}$ and G_{thresh} = 0.01 $G_{eq,\,c}$ were the definitions of the maximum energy release rate and the lower limit, respectively. $G_{eq,\,c}$ stands for the critical equivalent strain energy release rate, where the following mode-mix criterion (using the linear power law model) was used to calculate it.

$$\frac{G_{eq}}{G_{eq,c}} = \left(\frac{G_1}{G_{1c}}\right)^{\alpha_1} + \left(\frac{G_2}{G_{2c}}\right)^{\alpha_2} + \left(\frac{G_3}{G_{3c}}\right)^{\alpha_3} \quad (2)$$

The opening (Mode I), first shear (Mode II), and second shear (Mode III) critical energy release rates in this model are represented by the symbols G_{1c}, G_{2c}, and G_{3c}, respectively. In the analysis, it is assumed that the coefficients α_1, α_2 and α_3 have a value of 1.0.

The fatigue fracture in the structure is measured during the low-cycle fatigue study by ΔG, which is the difference in energy release rates between the minimum and maximum loads. The Paris Law, which is written as $da/dN = c_3\Delta G^{c_4}$, was used to calculate the progress rate of the crack per cycle. The crack length is denoted by the letter a, the cycle number is N, and the material constants are c_3 and c_4 [12]. In order to appropriately depict the beginning and progression of the crack, it is crucial to satisfy the condition $G_{pl} > G_{max} > G_{thresh}$ in the computations.

Following the start of a crack, the following steps are taken: one element was released at the interface at the end of each cycle N, allowing the software to advance the crack length (a_N) progressively from the current cycle to $a_{N+\Delta N}$. ΔN_j, where j is the node that corresponds to the crack tip and N is the number of cycles required to produce failure in each interface element at the crack tip. The determined node spacing at the interface elements close to the crack tips ($\Delta a_{Nj} = a_{N+\Delta N} - a_N$) and the material constants c_3 and c_4 were used in this calculation. The goal of the analysis was to release one or more interface elements at the end of each stable loading cycle. Thus, ΔN_{min} = min (ΔN_j), which indicates the number of cycles necessary for the crack to propagate across its element length, Δa_{Nmin} = min (Δa_{Nj}), was found to be the element that required the fewest cycles for

propagation. As a result, zero stiffness and constraint were achieved when the element requiring the fewest cycles was found to be suitable for release. According to [12], with the interface element released during the next cycle, a new relative fracture energy release rate was computed for the interface elements at the crack tip.

The material constants used in the simulations are listed in Table 1. They are mainly the elastic modulus, Poisson's ratio, tensile strength, the critical energy release rates in different modes (G_{1c}, G_{2c} and G_{3c}), and the material constants used in the Paris Law (c_3 and c_4).

Table 1. The material parameters for EN 10,130 low-carbon steel used in the simulations.

[13,14]			[15]		
***E* (MPa)**	***v***	***TS* (MPa)**	**G_{1c}, G_{2c}, G_{3c} (N/m)**	**c_3**	**c_4**
210,000	0.3	326	6500	7.5×10^{-8}	1.75

When T and $-T$ were applied during cyclic torsional loading, the spot-welded assembly's deformed shape was recorded, as shown in Figure 4.

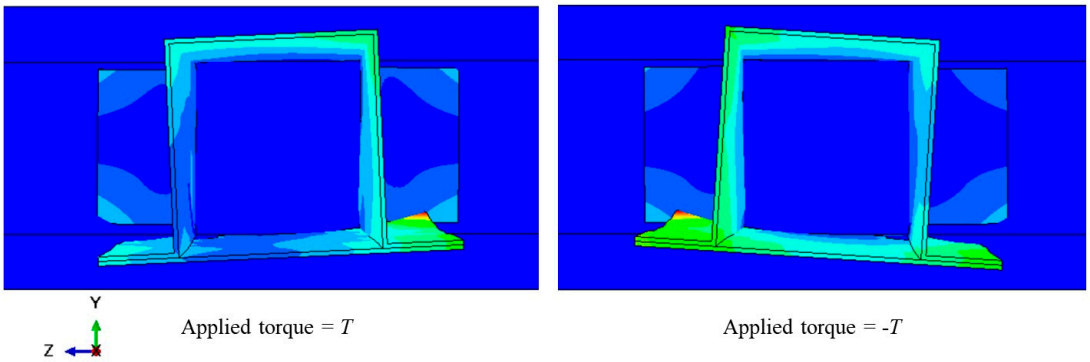


Figure 4. Deformed shape of the spot-welded assembly when T (**left**) and $-T$ (**right**) was applied during cyclic torsional loading (for improved visual aid, the deformation was scaled ten times).

3. Results and Discussion

This section presents first the numerical model's validation utilizing the assembly's failure cycles (N_f) that were obtained experimentally. The influence of various parameters was further examined, including the nugget diameter, the thickness of the assembled parts, the applied torque, the base presence concerning N_f and the location and sequential propagation of crack initiation. Discussions that were pertinent were also included.

3.1. Validation of the Numerical Model

For the validation of the developed XFEM model, the experimental data presented in (Dincer, 2005 [14]) were used. The spot-welded assembly was investigated in two different configurations. In the first configuration, the nugget diameter and part thicknesses were 5.5 mm and 1.5 mm, respectively, while in the second configuration, they were 6.5 mm and 2.0 mm. A 480 Nm. cyclic torsional loading was applied to the assembly. Table 2 displays the N_f values obtained through numerical analysis and experimental observation. The extension of t from 1.5 mm to 2.0 mm led to an increase in failure cycles from 37,290 to 96,000 experimentally; however, these values were 31,967 and 87,446 cycles, respectively, in numerical analysis. A satisfactory comprehension was achieved. Numerical simulations indicate that the initial appearance and propagation of the crack, leading to the eventual collapse of the assembly, occurred in Part 1 around the spot weld connecting Parts 1 and 2 on the lower left side (see Figure 5). This is also in line with the experimentally obtained crack propagation as shown in Figure 6.

Table 2. Experimentally and numerically obtained failure cycles for two different cases.

			Experiments [14]	XFEM
t	***D***	***T***	N_f	
1.5 mm	5.5 mm	±480 Nm	37,290	31,967
2.0 mm	6.5 mm		96,000	87,446

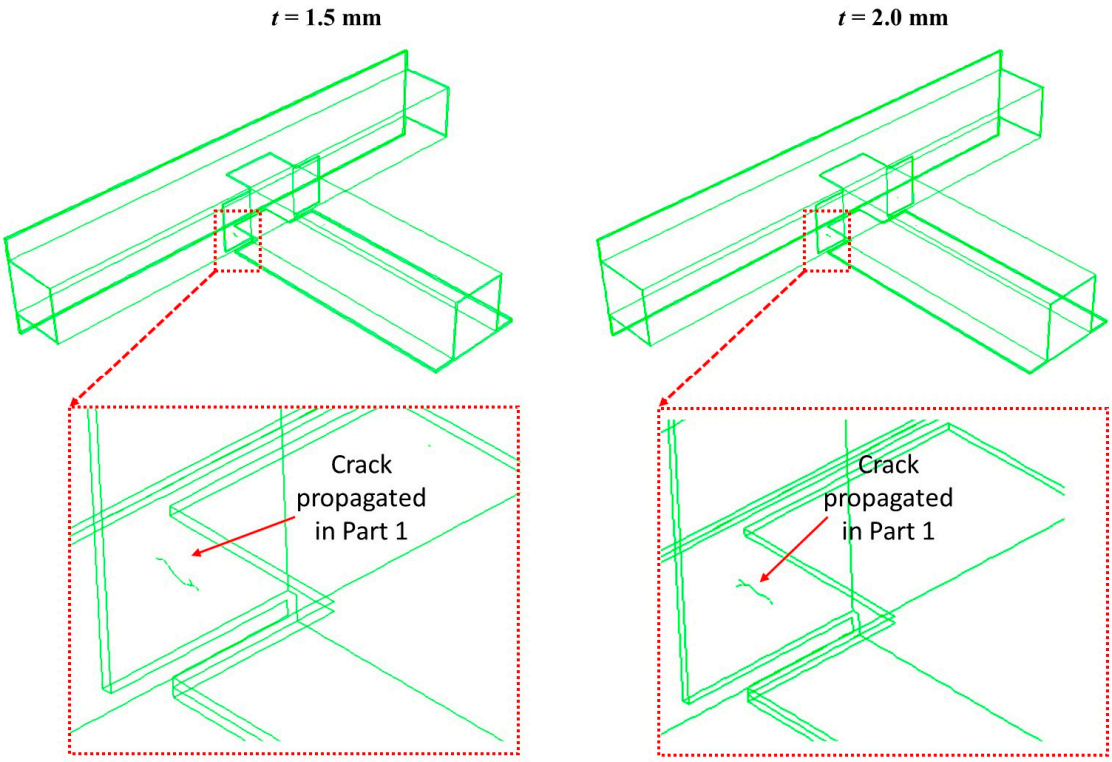


Figure 5. The shape of evolved cracks in the assembly for t = 1.5 and 2.0 mm upon N_f is reached for each configuration.

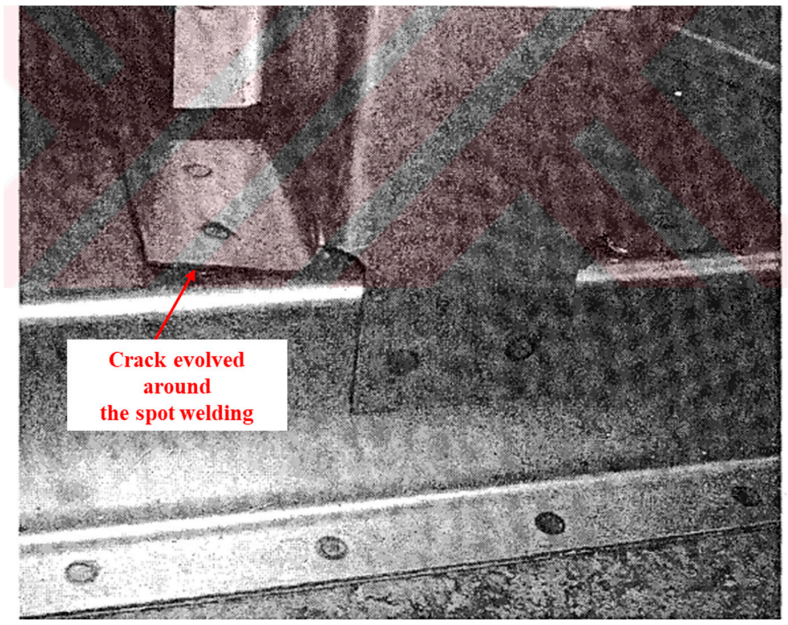


Figure 6. Experimentally observed crack pattern around the spot welds [14] (view from the bottom side of the assembly).

3.2. Influence of the Diameter of Spot Welds

One of the variables that could have an impact on the assembly's torsional performance is the spot weld's diameter. This investigation looked at three different scenarios in which D was adjusted from 4.5 mm to 6.5 mm with a 1.0 mm increase and t was maintained at 1.5 mm. The corresponding N_f and crack propagation rate (da/dN) values are shown in Figure 7. When D increased from 4.5 mm to 6.5 mm, there were 11,539, 37,290, and 79,283 cycles recorded, respectively, where N_f grew by 3.23 and 2.12 times while D climbed by 1.22 and 1.18 times, respectively. The average crack propagation rate was calculated for each configuration using $(a_f - a_0)/N_f$, where a_0 and a_f were the crack lengths at the end of static cycle and at $N = N_f$, respectively. It was observed to decrease from 6.79×10^{-4} mm/cycle to 1.19×10^{-4} mm/cycle and around 5.7 times when D was increased from 4.5 to 6.5 mm.

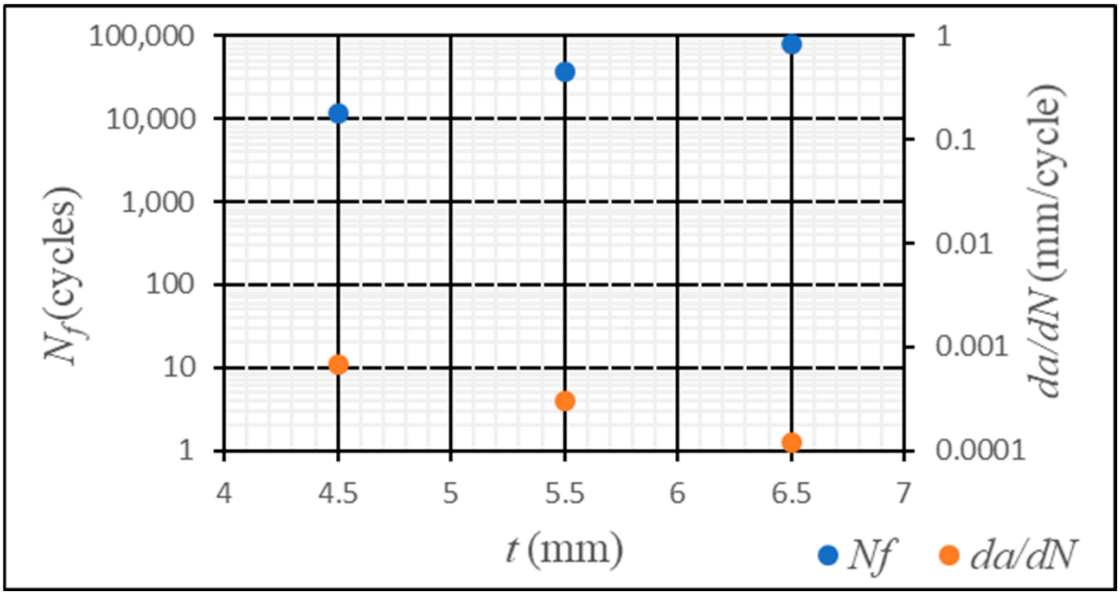


Figure 7. Numerically determined N_f and da/dN for various spot-weld diameters.

Figure 8 shows the resulting crack patterns for each configuration when N reaches 400,000 cycles. It was observed that regardless of the size of D, the crack emerged and expanded at the identical position in Part 1 around the spot weld connecting Parts 1 and 2 on the lower left side. After 400,000 cycles, the crack size increased to 34.01, 29.20, and 22.69 mm when D equaled 4.5, 5.5, and 6.5 mm, respectively. It was determined that when the nugget's diameter shrank, the crack propagated more quickly because the smaller spot-welding size could not assemble the parts adequately. Here, it was determined that the size of the spot weld significantly affected the fatigue performance of the structure. This is in line with what was shown in [16,17], where longer fatigue lives were achieved by larger nugget diameters because of the notch effect. This resulted in lower strains and stresses developing close to the spot-welding site, which decreased the likelihood that fractures would emerge.

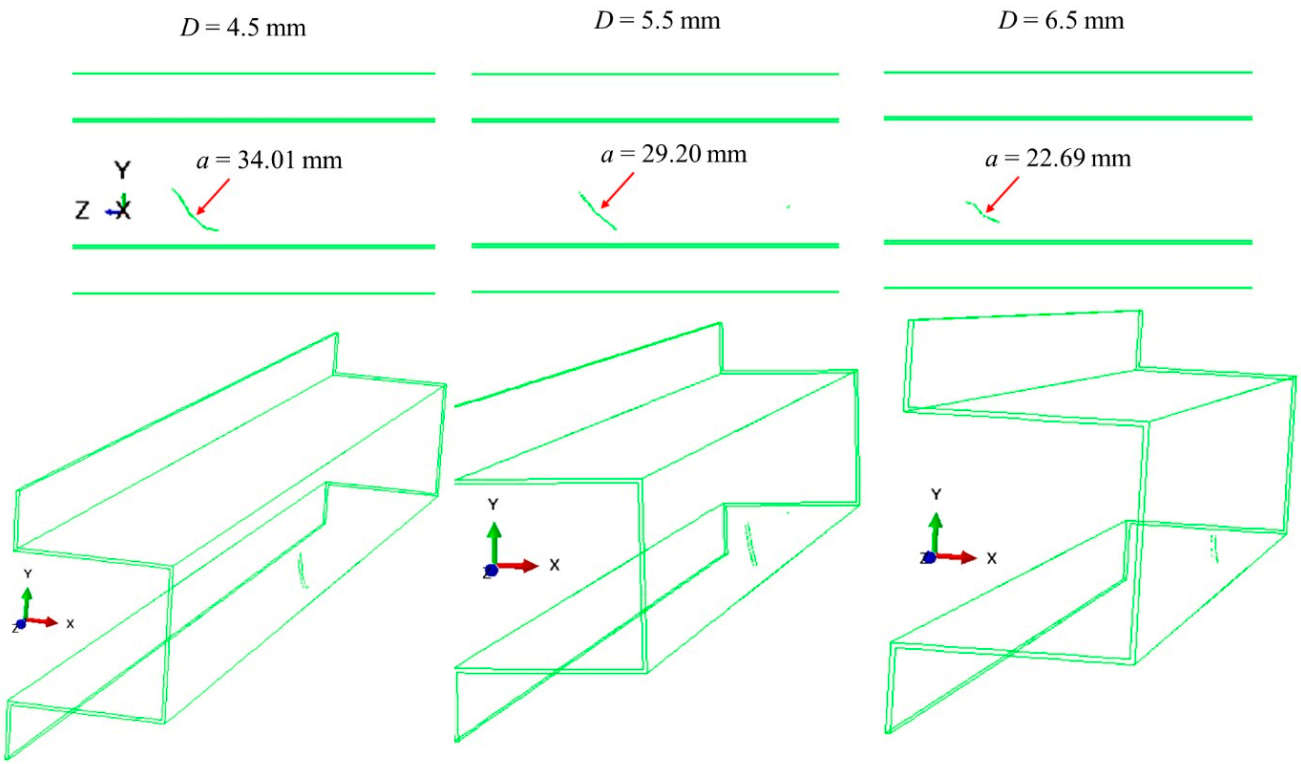


Figure 8. The depiction of the cracks that spread in Part 1 of the assembly for different diameters of spot welds at N = 400,000.

3.3. Influence of Thickness

Second, an analysis was conducted to determine the impact of the thickness of the components of the assembly on the spot-welded box's torsional fatigue life. This size was increased from 1.0 mm to 2.0 mm in increments of 0.5 mm. Figure 9 presents the obtained N_f values, with 9693, 37,290 and 10^6 cycles, respectively. Figure 10 displays the cracks observed at the end of the static analysis and after 10^6 cycles for the assembly with a thickness of 2.0 mm. Notably, these cracks are identical, indicating that they did not propagate further during the fatigue analysis, i.e., no fatigue failure was detected. Small cracks had formed prior to fatigue failure at various points across Parts 1–3, contrasting with the absence of crack formation at the location observed for a thickness of 1.5 mm (see Figure 8). In this investigation, a fatigue life exceeding 10^6 cycles was regarded as reaching the run-out threshold. This finding indicated that by increasing the thickness, fatigue failure in such a structure subjected to torsional loading may be eliminated. On the other hand, when t = 1.0 mm was used in the parts of the assembly, the N_f decreased by more than 3.8 times when compared to that of t = 1.5 mm. The structure became weaker in that case, and the applied torque of ±480 Nm. caused the cracks to propagate quickly (the average da/dN increased more than 3 times from 3.02×10^{-4} to 9.63×10^{-4} mm/cycle), resulting in a reduced fatigue life. Figure 11 presents the resulting crack patterns after N_f is reached for t = 1.0 mm. It was observed that multiple cracks propagated in different parts of the assembly, completely different than that of t = 1.5 mm (see Figure 8). It was concluded that the thickness affected the failure pattern of the assembly subjected to torsional fatigue significantly.

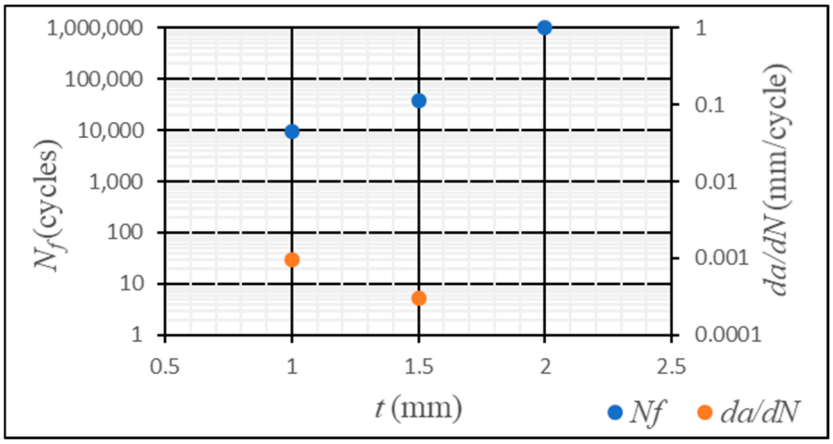


Figure 9. N_f and da/dN values obtained for different thicknesses of the parts.

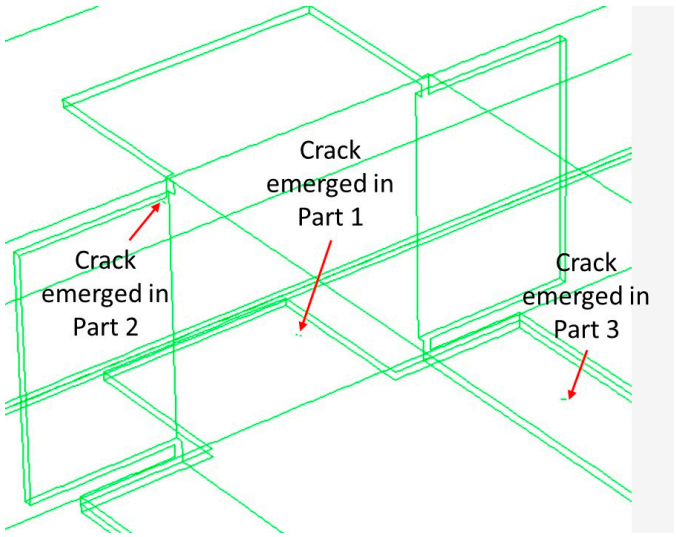


Figure 10. The depiction of the cracks that spread in the assembly for t = 2.0 mm at N = 0 and 10^6 cycles.

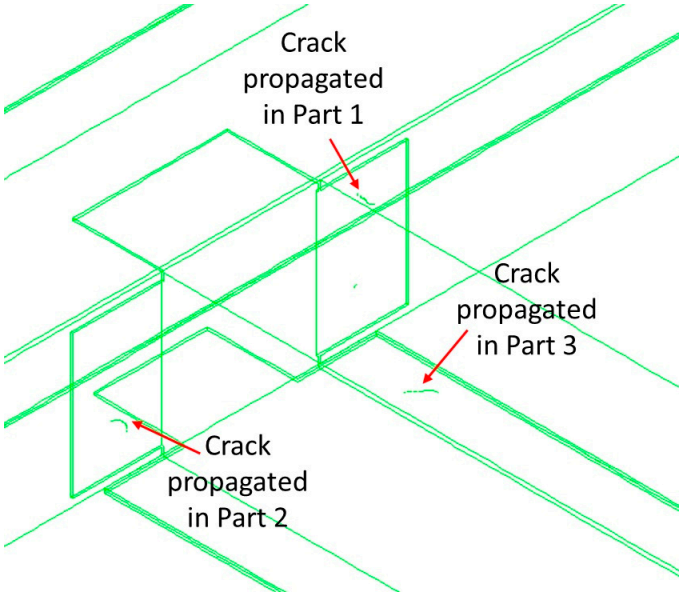


Figure 11. The depiction of the cracks that spread in the assembly for t = 1.0 mm at $N = N_f$.

3.4. Effects of Torque Amount and the Presence of Base for Part 1

Lastly, the influence of torque magnitude and presence of Part 4 on the fatigue performance of the assembly was investigated. Here, the T was changed into ±360 Nm and ±600 Nm from the reference value of ±480 Nm. Also, in one of the simulations, Part 4 was removed from the assembly. Table 3 shows the respective resulting N_f and da/dN values. It was observed that N_f increased almost 2 times for T = ±360 Nm when compared to the reference value, whereas the fatigue life became less than half of it for T = ±600 Nm (decreased to 16,928 cycle from 37,290 cycle). The respective average da/dN values were 1.08×10^{-4} and 5.76×10^{-4} mm/cycle. On the other hand, the assembly's fatigue life plummeted to just 2644 cycles with a very high average crack spread rate, with 2.79×10^{-4} mm/cycle, when the supporting foundation, Part 4, was removed, demonstrating its critical role in the structure's improved fatigue performance. Figure 12 presents the resulting crack patterns for the studied cases. When Part 4 was removed or T was altered from its reference value to another, no discernible difference was seen; however, for T = ±600 Nm, the main crack appeared in Part 1 around the spot weld connecting Parts 1 and 2 on the bottom right side rather than the left. This discrepancy can be disregarded because the structure is symmetric with respect to the XY plane.

Table 3. N_f and da/dN values obtained for different torque values and configurations of the assembly.

T (Nm)	N_f	da/dN (mm/Cycle)
±360	72,586	1.08×10^{-4}
±480	37,290	3.02×10^{-4}
±480 (without Part 4)	2644	2.79×10^{-3}
±600	16,928	5.76×10^{-4}

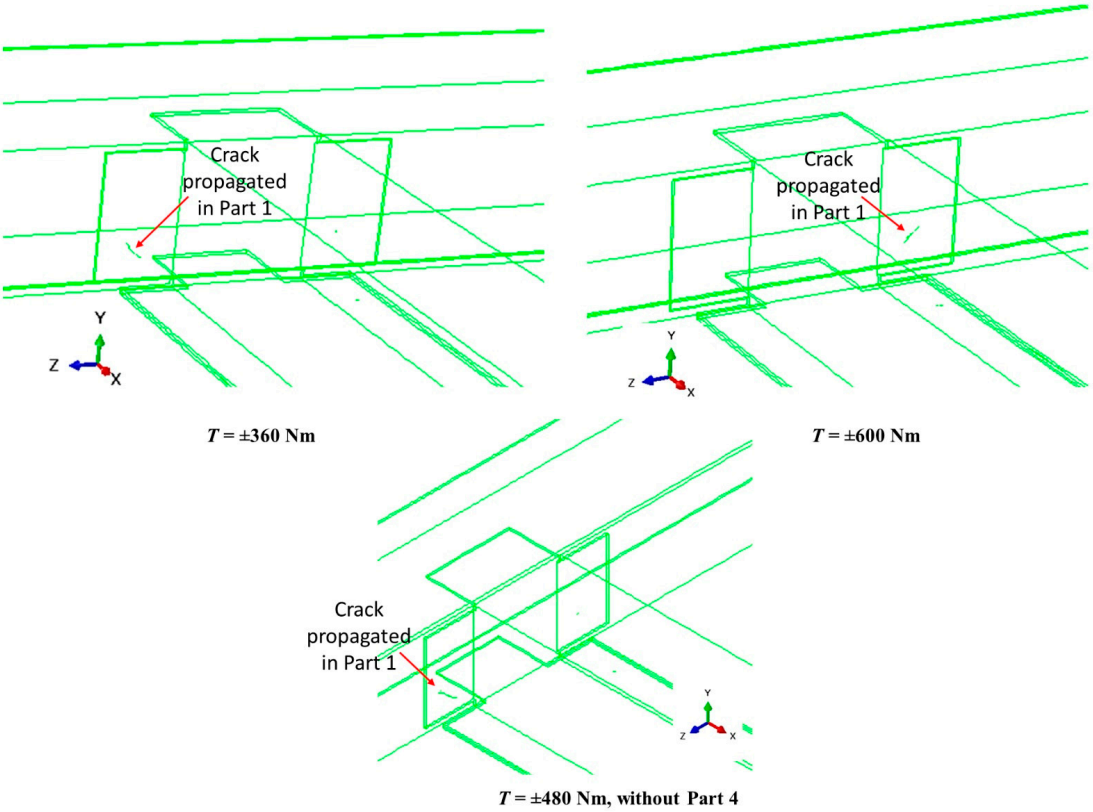


Figure 12. The depiction of the cracks that spread in the assembly for different torque values and configurations of the assembly at $N = N_f$.

4. Conclusions

This study examined the fatigue failure of the T-profile assembly under torsional loading by considering several key parameters that included the magnitude of torque applied, thickness of assembly components, and spot-weld diameter. Crack propagation was simulated using the XFEM modeling approach, with the model's accuracy confirmed against experimental data from previous studies. The following conclusions were drawn.

Increasing the spot weld diameter from 4.5 mm to 6.5 mm significantly enhanced the assembly's torsional performance. The number of cycles N_f increased 3.23 times, while the crack propagation rate da/dN decreased by approximately 5.7 times. Regardless of weld size, cracks formed at the same location but propagated faster with smaller diameters due to inadequate assembly. Lower strains and stresses from larger diameters improved fatigue performance and decreased the chance of fracture.

When the thicknesses of the parts were changed from 1.5 mm to 1.0 mm, the N_f decreased by more than 3.8 times, while the average da/dN increased more than 3 times. For t = 2.0 mm, an infinite fatigue life was achieved.

When the T was changed from $\pm$360 into $\pm$600 Nm, the N_f decreased by 4.28 times, while the average crack propagation rate increased 5.33 times. It was found that one of the assembly's supporting components greatly enhanced the structure's fatigue performance, with the N_f rising by more than 14 times.

Author Contributions: Conceptualization, M.D.; Methodology, M.D. and F.K.; Validation, M.D.; Formal analysis, M.D.; Investigation, M.D.; Writing—original draft, M.D.; Writing—review & editing, F.K. All authors have read and agreed to the published version of the manuscript.

Funding: The APC was funded by the American University of the Middle East, Kuwait.

Institutional Review Board Statement: Not applicable.

Informed Consent Statement: Not applicable.

Data Availability Statement: Data sets generated during the current study are available from the corresponding author on reasonable request.

Conflicts of Interest: The authors of this manuscript declare that there are no conflicts of interest regarding the publication of this paper. All research was conducted without any financial or personal relationships that could inappropriately influence or bias the work presented. We affirm that the results and conclusions of this study are solely based on objective scientific inquiry.

References

1. Lipiäinen, K.; Ahola, A.; Javaheri, V.; Björk, T. Ultimate tensile capacity of hot-dip galvanized ultra-high-strength steel cut edges and welded joints. *Weld. World* **2023**, *67*, 2779–2789. [CrossRef]
2. Verspeek, S.; Ribbens, B.; Maldague, X.; Steenackers, G. Spot weld inspections using active thermography. *Appl. Sci.* **2022**, *12*, 5668. [CrossRef]
3. Ruiz, H.; Osawa, N.; Rashed, S. Study on the stability of compressive residual stress induced by high-frequency mechanical impact under cyclic loadings with spike loads. *Weld. World* **2020**, *64*, 1855–1865. [CrossRef]
4. Kardomateas, G.A. Spot weld failure from buckling-induced stressing of beams under cyclic bending and torsion. *Eng. Fract. Mech.* **1992**, *42*, 519–530. [CrossRef]
5. Janardhan, G.; Mukhopadhyay, G.; Dutta, K. Failure mechanism of resistance spot-welded DP600 steel under high cycle fatigue. *Mater. Today: Proc.* **2022**, *59*, 1666–1671. [CrossRef]
6. Ertas, A.H.; Akbulut, M. Experimental study on fatigue performance of resistance spot-welded sheet metals. *Int. J. Adv. Manuf. Technol.* **2021**, *114*, 1205–1218. [CrossRef]
7. Duran, E.T.; Demiral, M. Comparing and validating the numerical modeling of spot-welded fatigue failure using FEM and XFEM methods for HCF. *Eng. Fail. Anal.* **2024**, *158*, 108049. [CrossRef]
8. Qian, C.; Ghassemi-Armaki, H.; Shi, L.; Kang, J.; Haselhuhn, A.S.; Carlson, B.E. Competing fracture modes in Al-steel resistance spot welded structures: Experimental evaluation and numerical prediction. *Int. J. Impact Eng.* **2024**, *185*, 104838. [CrossRef]
9. Aghabeigi, M.; Hassanifard, S.; Hashemi, S.M. Evaluation of different strain- based damage criteria for predicting the fatigue life of friction stir spot-welded joints under multi-axial loading conditions. *Proc. Inst. Mech. Eng. Part L J. Mater. Des. Appl.* **2020**, *234*, 156–166. [CrossRef]

10. Oh, G.; Umezawa, A. Combined loading effect on high cycle fatigue fracture behaviors of a stainless steel welded structure of elbow and socket. *Int. J. Fatigue* **2023**, *175*, 107777. [CrossRef]
11. Elitas, M.; Goktas, M.; Acarer, M.; Demir, B. Finite element modelling of the fatigue damage in an explosive welded Al-dual-phase steel. *Mater. Test.* **2023**, *65*, 787–801. [CrossRef]
12. Dassault Systèmes. *Abaqus Documentation*; Dassault Systèmes: Providence, RI, USA, 2021.
13. Duran, E.T. Finite element based Multi-Axial low cycle fatigue analyses of Spot-Welded components and correlation with tests. *Eng. Fail. Anal.* **2022**, *132*, 105899. [CrossRef]
14. Dincer, S. A Comparative Study on the Finite Element Models for Spot Welds and Their Verification. Master's Thesis, Istanbul Technical University, İstanbul, Turkey, 2005. [CrossRef]
15. Gupta, R.S.; Xin, H.; Veljkovic, M. Fatigue crack propagation simulation of orthotropic bridge deck based on extended finite element method. *Procedia Struct. Integr.* **2019**, *22*, 283–290. [CrossRef]
16. Ertas, A.H.; Sonmez, F.O. A parametric study on fatigue strength of spot-weld joints. *Fatigue Fract. Eng. Mater. Struct.* **2008**, *31*, 766–776. [CrossRef]
17. Demiral, M.; Duran, E.T. Torsional Fatigue Performance of a Spot-Welded Structure: An XFEM Analysis. *Appl. Sci.* **2024**, *14*, 9593. [CrossRef]

Disclaimer/Publisher's Note: The statements, opinions and data contained in all publications are solely those of the individual author(s) and contributor(s) and not of MDPI and/or the editor(s). MDPI and/or the editor(s) disclaim responsibility for any injury to people or property resulting from any ideas, methods, instructions or products referred to in the content.